Supplementary information

Mapping morphological identifiers for distinct conformations via protein translocation current in nanopore

Mingkun Zhang[1,2,3,4], Shenbao Chen[1,2], Jinrong Hu[1,2], Qihan Ding[1,2], Linda Li[1,2], Shouqin Lü[1,2,], Mian Long[1,2,*]*

[1] Center of Biomechanics and Bioengineering, Key Laboratory of Microgravity (National Microgravity Laboratory), Beijing Key Laboratory of Engineered Construction and Mechanobiology, and CAS Center for Excellence in Complex System Mechanics, Institute of Mechanics, Chinese Academy of Sciences, Beijing, 100190, China.

[2] School of Engineering Science, University of Chinese Academy of Sciences, Beijing, 100049, China.

[3] Chongqing Engineering Research Center of High-Resolution and Three-Dimensional Dynamic Imaging Technology, Chongqing Institute of Green and Intelligent Technology, Chinese Academy of Sciences, Chongqing, 400714, China.

[4] Chongqing School, University of Chinese Academy of Sciences, Chongqing 400714, China.

[*] Correspondence: Prof. Shouqin Lü (E-mail: lsq@imech.ac.cn) or Prof. Mian Long (E-mail: mlong@imech.ac.cn), Institute of Mechanics, Chinese Academy of Sciences, No. 15 North 4th Ring Road, Beijing 100190, China.

Contents

Supplementary Notes

Supplementary Note 1. Spheroidal approximation of a protein in nanopore-based identification

Considering two typical shapes of a particle, oblate and prolate, with respective length in rotational axis A and the diameter in equatorial axis B (**Figure S5**), the particle volume in Equation 3 is termed as $\Lambda=\pi AB^2/6$. Non-spheres alter the electric field to a certain extent depending on their orientation relative to the direction of the field. Thus, an electrical shape factor of the spheroid, f, is estimated as a function of a particle's orientation, or more specifically, the angle between the rotational axis and the electric field direction, θ [1, 2]:

$$f(\theta) = f_{\perp} + (f_{\parallel} - f_{\perp})\cos^2\theta \quad (S1)$$

where $f_{\perp}$ and $f_{\parallel}$ are the electrical shape factors when the rotational axis is perpendicular to and parallel with the electric field, respectively. Equation S1 implies that the shape factor for any direction ranges between the values of $f_{\perp}$ and $f_{\parallel}$. These two factors are related to the well-described depolarization factors for ellipsoids $\zeta_{\perp}$ and $\zeta_{\parallel}$, which are a function of the ratio of ellipsoidal length to diameter, $\eta = A/B$ [1, 3-5]:

$$f_{\perp} = \frac{1}{1-\zeta_{\perp}} \quad (S2)$$

$$f_{\parallel} = \frac{1}{1-\zeta_{\parallel}} \quad (S3)$$

$$\zeta_{\parallel} = \frac{1}{\eta^2-1}\left[\frac{\eta}{\sqrt{\eta^2-1}}\ln\left(\eta+\sqrt{\eta^2-1}\right)-1\right],\ (\eta>1)$$

$$\zeta_{\parallel} = \frac{1}{1-\eta^2}\left[1-\frac{\eta}{\sqrt{1-\eta^2}}\cos^{-1}\eta\right],\ (\eta<1) \quad (S4)$$

$$\zeta_{\parallel} + 2\zeta_{\perp} = 1 \quad (S5)$$

When the ellipsoidal size of the particle approaches the diameter of the pore, the electric field

in the pore is additionally distorted in a non-linear increase in the resistance with increscent particle volume [6, 7]. Thus, Equation 3 needs to be modified as [5, 8]:

$$\frac{\Delta I}{I_0} == \frac{4\Lambda f}{\pi d_p^2 l_p} S(\Lambda) = \frac{2AB^2 f}{3d_p^2 l_p}\left[1 - 0.8\left(\frac{A+B}{2d_p}\right)^3\right]^{-1} \quad (S6)$$

Here $S(\Lambda)$ is a correction factor which is usually taken into account when $(A+B)/2 > 0.5d_p$.

Equations S1-S6 illustrate that the relative blockade current of approximate spheroid of a protein is a function of the length A, diameter B and orientation angle θ. The shape factor $f_\perp$ and $f_\parallel$ are the two extremes of the maximal and minimal projected areas of the ellipsoid on the nanopore cross-section for approximate spheroid of protein. Thus, the two extreme orientations of each conformation with maximal and minimal projected areas in radial plane of the nanopore are obtained by rotating the crystal structure by 1° step around three coordinate directions (**Figure 1b**). The polar angle between other arbitrary orientation and the alternative extreme orientation along Z-axis is calculated respectively by the rotation matrix of the coordinates of protein atoms (**Figure 2a**). The orientation angle θ is the polar angle converted to a range of 0 to 90° due to the symmetry of the spheroid (**Figure S5**).

Supplementary Note 2. Calculation rationale of conductivity distribution

Radial conductivity distribution of the cylindrical nanopore

Following a method described previously [9-11], from the inner surface of the nanopore wall, the volume inside the nanopore is radially decomposed into successive coaxial cylindrical rings with 1-Å thickness each, sequentially extending to the symmetry axis. The ion concentration C_r in r^{th} ring shell is calculated as:

$$C_r = \frac{n_r}{N_A \cdot \Omega_r} \tag{S7}$$

where n_r is the number of ions or water molecules in r^{th} ring shell, Ω_r is the volume of the r^{th} cylindrical ring shell, and N_A is the Avogadro's number. The mean migrating velocity v_r of ions in r^{th} ring shell is calculated as:

$$v_r = \frac{\sum_{j=1}^{m-1} \frac{\sum_{i=1}^{n_r} \frac{z_{i,j+1} - z_{i,j}}{\Delta t}}{n_r}}{m-1} \tag{S8}$$

where $z_{i,j+1}$ and $z_{i,j}$ indicate the Z-axis coordinates (or the coordinates of other axis along which the electric field is applied) of i^{th} ion in $(j+1)^{th}$ and j^{th} frames of the trajectory, Δt denotes the time interval between the consecutive frames, and m stands for the number of total frames of the MD trajectory. The conductivity in r^{th} ring shell is thus calculated as:

$$\sigma_r = F\left(C_{r+}\mu_{r+} + C_{r-}\mu_{r-}\right) = F\left(C_{r+}v_{r+} + C_{r-}v_{r-}\right)E^{-1} \tag{S9}$$

where $C_{r+(-)}$ is the concentration of potassium or chloride ions in r^{th} ring shell, $\mu_{r+(-)}$ and $v_{r+(-)}$ are the mean ionic mobility and mean ionic velocity of potassium or chloride ions along the external electric field E in r^{th} ring shell, respectively, and F is the total charge of 1 mole electrons.

Conductivity distribution with a distance from the protein

The volume of electrolyte region around the protein is decomposed into serial 1-Å thick shells with protein-enveloped shapes, each of which is composed of the discrete meshes with the same distance from the protein surface. The distance from the center of each cubic mesh to the nearest protein surface and the number density of ions or water molecules in each mesh are both determined by the VolMap plugin of VMD. The ion concentration in each shell can be determined from the distance and density maps created via VolMap plugin above. Meanwhile, the ion velocity in each shell is calculated from the ion coordinates over time. Finally, the conductivity distribution around the protein is obtained by integrating the concentration and velocity profiles in successive partitioned shells.

Supplementary Note 3. Discrete model for calculating conductivity of nanopore system

Following a method described previously [9], after decomposing the nanopore space into sequential 1-Å thick coaxial cylindrical rings, each ring shell is further divided into a collection of cylindrical ring layers with 1 Å-thickness along the cylindrical axis (**Figure S11**). For the nanopore filled with plain electrolyte, the conductivity σ_{ij} of cube *j* in layer *i* is determined by the distance to the pore wall via Equation 4. For the nanopore blocked by a protein, the conductivity σ_{ij} of each cubic mesh within the modulation range of the protein-occupied region is updated by the distance to the nearest protein surface via Equation 5.

The conductance of the cubic mesh is calculated as

$$G_{ij} = \frac{\sigma(r_{ij})S_{ij}}{l_{ij}} \quad (S10)$$

where l_{ij} and S_{ij} are the length and the cross-sectional area of the cube, respectively. The conductance G_r of each ring shell of 1-Å thickness yields:

$$G_{ir} = \sum G_{ij}, \frac{1}{G_r} = \sum_{i=1}^{N} \frac{1}{G_{ir}} \quad (S11)$$

where G_{ir} denotes the conductance of i^{th} layer in r^{th} ring shell, and *N* stands for the number of ring layers along the cylindrical axis. The conductance *G* of the entire nanopore is summed up:

$$G = \sum_{r=1}^{M} G_r \quad (S12)$$

where *M* is the number of coaxial cylindrical rings. Note that this model does not take into account the effect of charges on pore wall, which is justified by the features of the all-atom model [12] used in this work.

Supplementary Figures

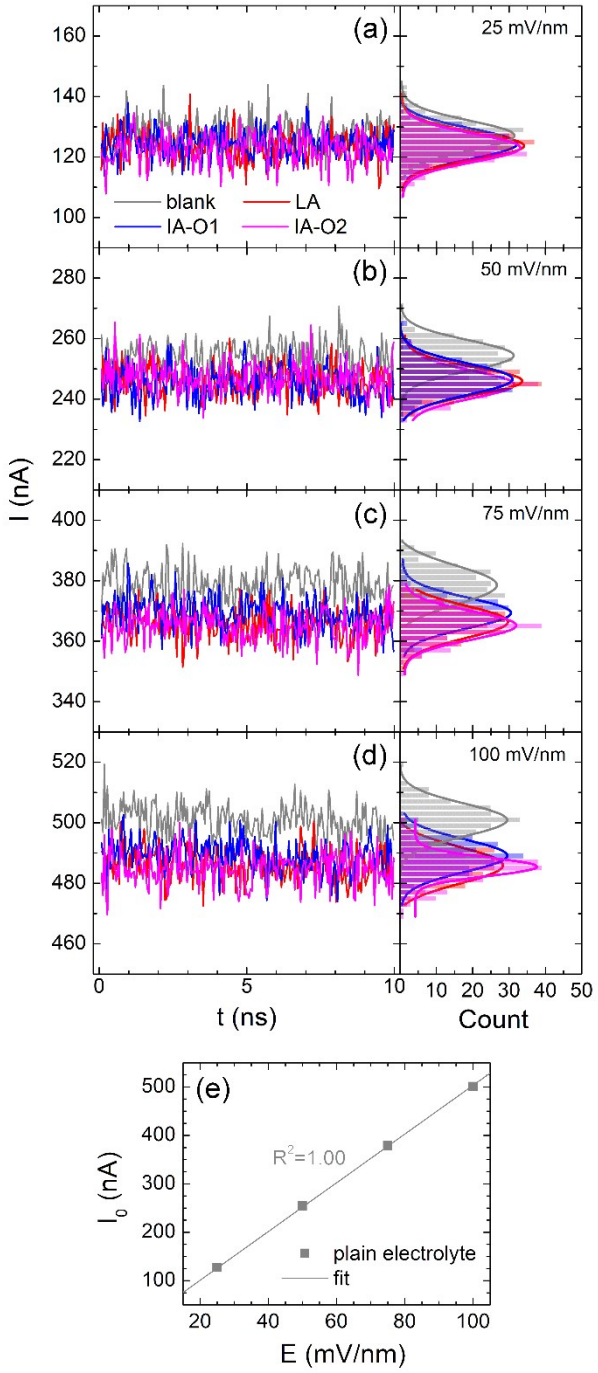

Figure S1. Time-lapsed samplings and Gaussian fittings of ionic currents computed from MD simulations in a 30-nm diameter nanopore at *E*=25 (a), 50 (b), 75 (c) or 100 mV/nm (d). The electric field pointed upward along the symmetry axis of cylindrical channel filled with 1 M KCl electrolyte. *Gray*, *red* or *blue*, *magenta trace* denotes the ionic current recorded

in the protein-free nanopore, the nanopore blocked by a low-affinity (*LA*) or an intermediate-affinity (*IA*) $\alpha_x\beta_2$ of two different orientations with small (*IA-O1*) and large (*IA-O2*) projected areas in the radial plane of the nanopore, respectively. The histograms of the current traces (*bars*) and the corresponding Gaussian fittings (*curves*) are also shown in the right. The current traces were sampled every 50 ps by Equation 7 from a single simulation. (**e**) Ionic current I_0 versus electric field intensity E in a protein-free nanopore. Each current point was obtained from the median of Gaussian fitting for all-points histogram in a 10-ns duration as described in panel **a-d**. *Solid line* denotes the fitting from Equation 1 in the main text, and R^2 is the determination coefficient (R-squared) for the fitting.

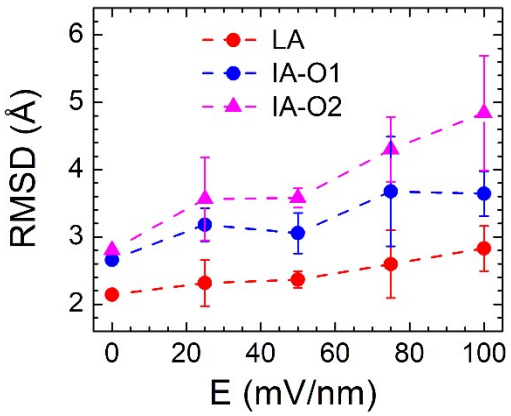

Figure S2. Effects of electric fields on conformational changes of $\alpha_x\beta_2$ in a 30-nm diameter nanopore. The average root-mean-square deviation (RMSD) of a 10-ns sampling was considered to be the averaged RMSDs of all the 200-frame trajectories compared with the initial frame. The data point and error bar are the mean and the standard deviation (SD) of two average RMSDs from two independent 10-ns simulations.

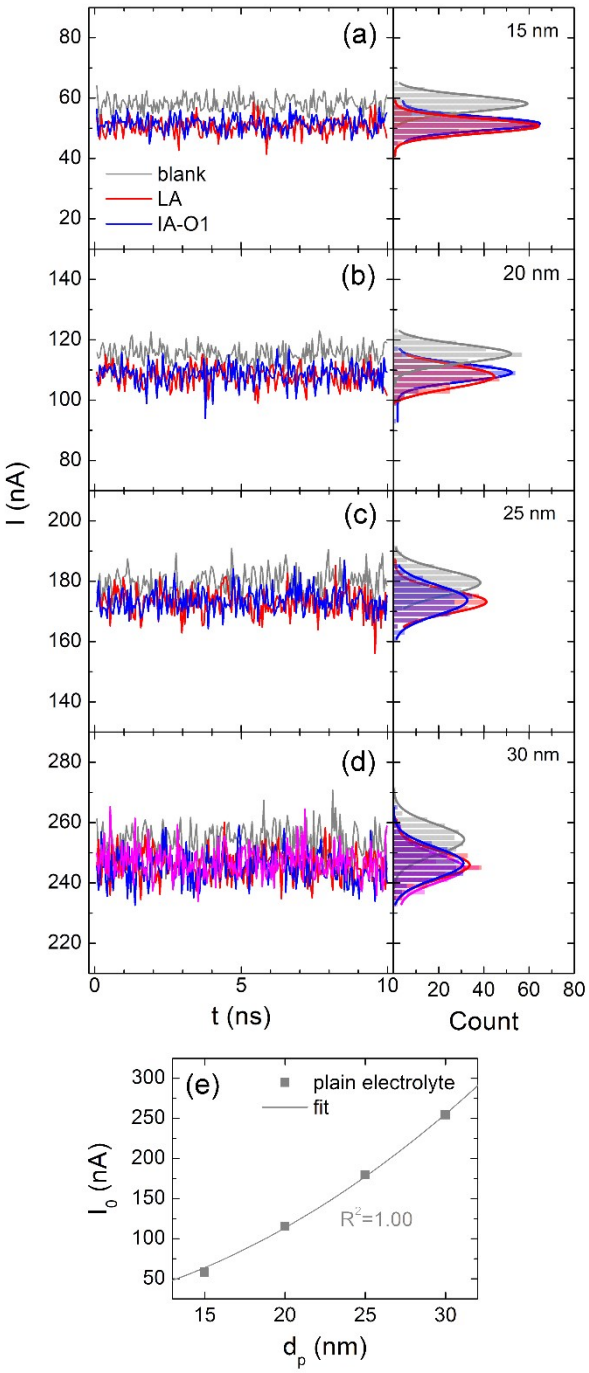

Figure S3. Time-lapsed samplings and Gaussian fittings of ionic currents computed from MD simulations at *E*=50 mV/nm in a 15 (a), 20 (b), 25 (c) or 30-nm (d) diameter nanopore. The electric field pointed upward along the symmetry axis of cylindrical channel filled with 1 M KCl electrolyte. *Gray*, *red* or *blue trace* denotes the ionic current recorded in the protein-free nanopore, the nanopore blocked by a *LA* $\alpha_x\beta_2$ or an *IA* $\alpha_x\beta_2$ with small projected area (*IA-O1*). The histograms of the current traces (*bars*) and the corresponding Gaussian fittings (*curves*) are shown in the right. The current traces were sampled every 50 ps by Equation 7 from a single simulation. (**e**) Ionic current versus nanopore diameter d_p in a protein-free

nanopore. Each current point was obtained from the median of Gaussian fitting for all-points histogram in a 10-ns duration as described in panel **a**-**d**. *Solid line* denotes the fitting from Equation 1, and R^2 is the *R*-squared.

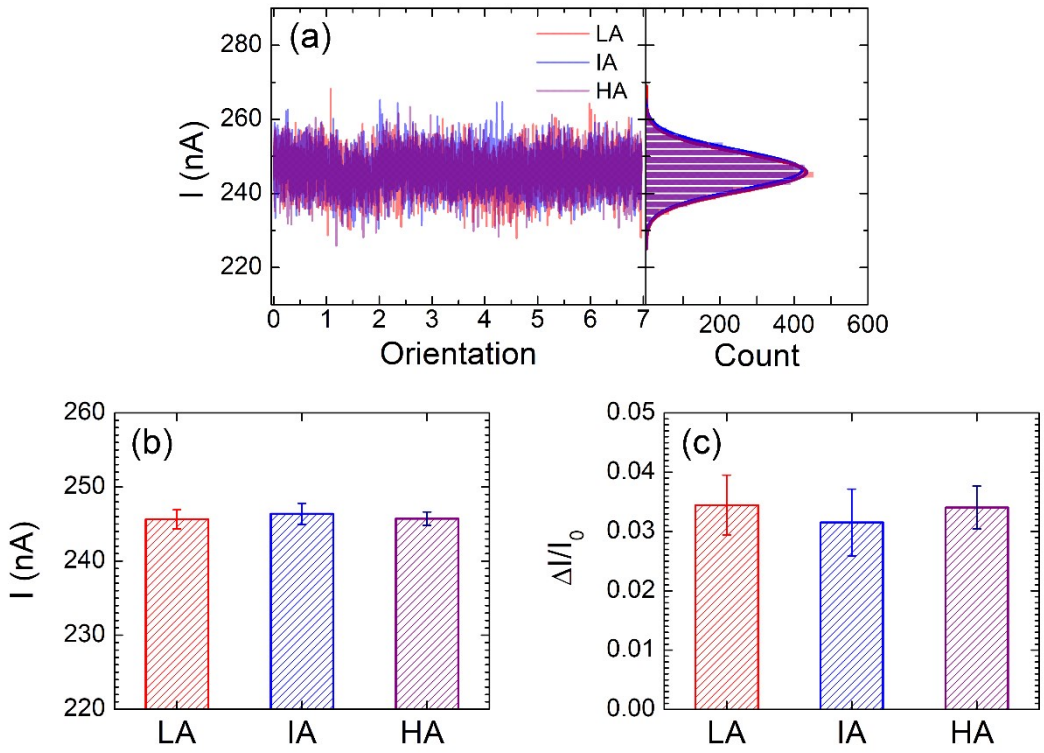

Figure S4. Conformational identification on the coupled conformation and orientation of $\alpha_x\beta_2$ placed inside a 30-nm diameter nanopore. (**a**) Ionic currents *I* recorded from MD simulations for three distinct conformations of $\alpha_x\beta_2$. *Red*, *blue* and *purple traces* denote the sampled currents of a *LA*, *IA* and high-affinity (*HA*) $\alpha_x\beta_2$, respectively, with seven different orientations for each conformation. Two independent simulations with 10-ns sampling duration and 50-ps sampling rate were performed for every orientation. For each conformation state, all histograms of the current traces (*bars*) and the corresponding Gaussian fittings (*curves*) are shown in the right. (**b-c**) Statistics of absolute (**b**) or relative (**c**) blockade current is presented as the mean value of the median currents of individual Gaussian fittings (*cf.* **Figures S1 and S3**) for all seven orientations with two independent simulations under each conformation. Error bar represents SD.

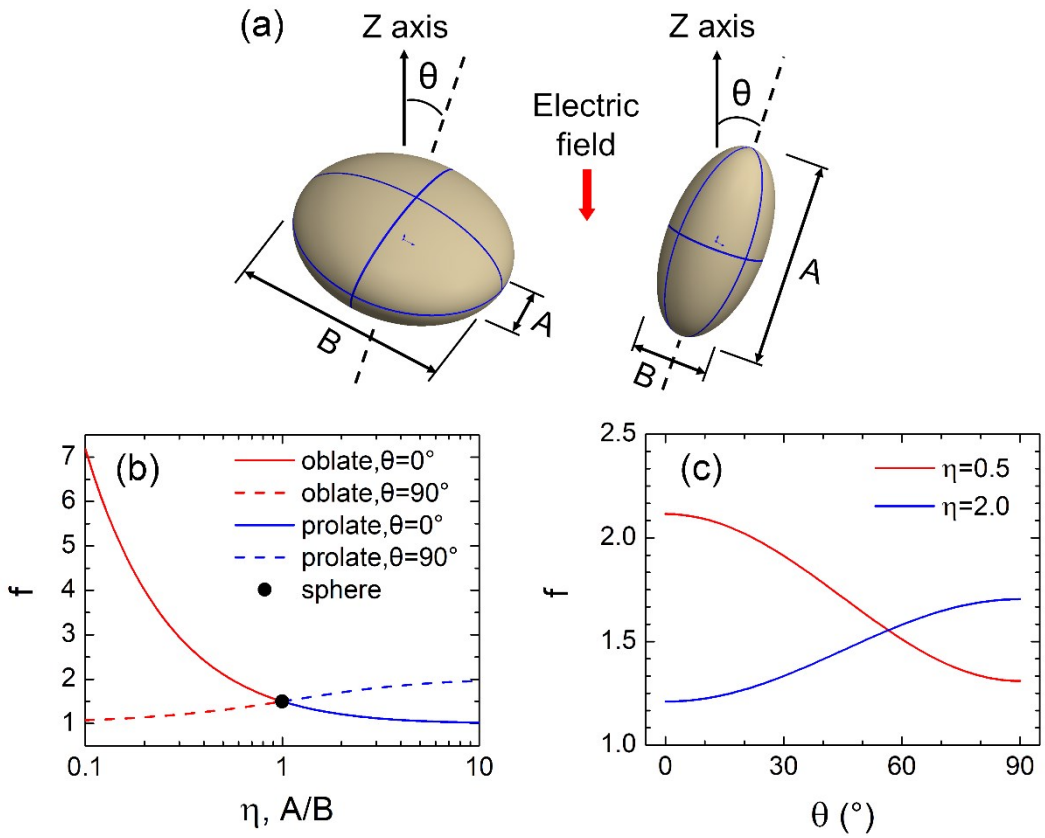

Figure S5. Schematics of the spheroidal approximation adopted from the literature 13. (**a**) Schematic of the two shapes of spheroid with a length-to-diameter ratio $\eta=A/B$, where A is the length in rotational axis and B is the diameter in equatorial axis. Here $\eta<1$ describes an oblate shape (η=0.5, *left*), η=1 denotes a spherical shape, and $\eta>1$ implies a prolate shape (η=2.0, *right*). For spheroidal approximation, the orientation angle θ is defined as the angle between the rotational axis and the direction of electric field. Given the symmetry of the spheroid, the θ value ranges from 0 to 90°. (**b**) Dependence of electrical shape factor f on η value at θ=0 or 90° (*lines*). f value for spherical shape is a constant of 1.5 (*solid point*). (**c**) The variations of the electrical shape factor f with orientation angle θ of two spheroids depicted in panel **a**. It is thus supposed that the orientation of the maximal or minimal projected area of the protein in the radial plane of the nanopore corresponds to the extreme orientation of 0° in the spheroidal approximation, as illustrated in **Figure 2**.

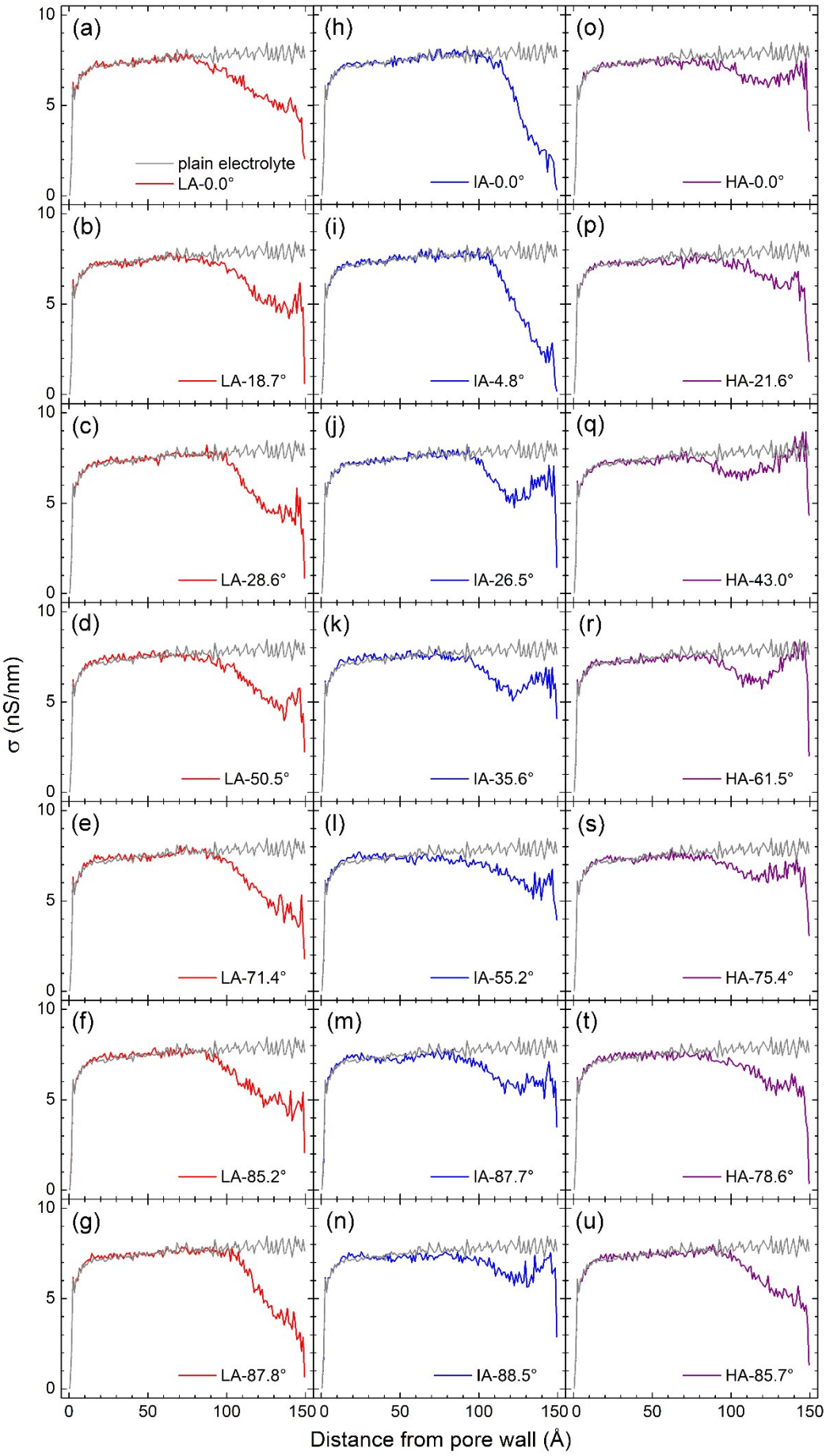
(a)
plain electrolyte
LA-0.0°
(h)
IA-0.0°
(o)
HA-0.0°
(b)
LA-18.7°
(i)
IA-4.8°
(p)
HA-21.6°
(c)
LA-28.6°
(j)
IA-26.5°
(q)
HA-43.0°
(d)
LA-50.5°
(k)
IA-35.6°
(r)
HA-61.5°
(e)
LA-71.4°
(l)
IA-55.2°
(s)
HA-75.4°
(f)
LA-85.2°
(m)
IA-87.7°
(t)
HA-78.6°
(g)
LA-87.8°
(n)
IA-88.5°
(u)
HA-85.7°
σ (nS/nm)
Distance from pore wall (Å)
0
5
10
50
100
150

Figure S6. Radial conductivity distributions in the absence or presence of $\alpha_x\beta_2$ placed inside a 30-nm diameter nanopore at 50 mV/nm. (**a-u**) Values of radial conductivities of various orientation angles of *LA* (**a-g**, *red lines*), *IA* (**h-n**, *blue lines*) or *HA* (**o-u**, *purple lines*) $\alpha_x\beta_2$, compared with those in the absence of protein (*grey lines*). Data were acquired for seven orientations ranging from 0-90° from a 10-ns simulation each. The volume of nanopore was partitioned into a series of successive coaxial cylindrical rings with 1 Å thickness in the radial direction from the wall surface to the pore symmetrical axis (**Supplementary Note 2**). The conductivity in each cylindrical ring was calculated from the 200 frames sampled from 10-ns simulation in 1 M KCl electrolyte.

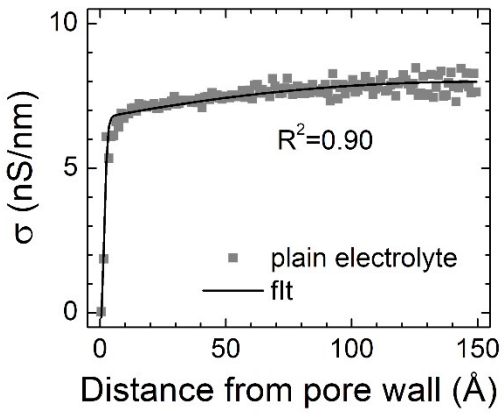

Figure S7. Radial conductivity σ of plain electrolyte in the nanopore versus the distance from the pore wall. The *grey squares* represent the data of the *grey line* in **Figure S6**. *Black line* denotes the fitting from Equation 4, and R^2 is the *R*-squared.

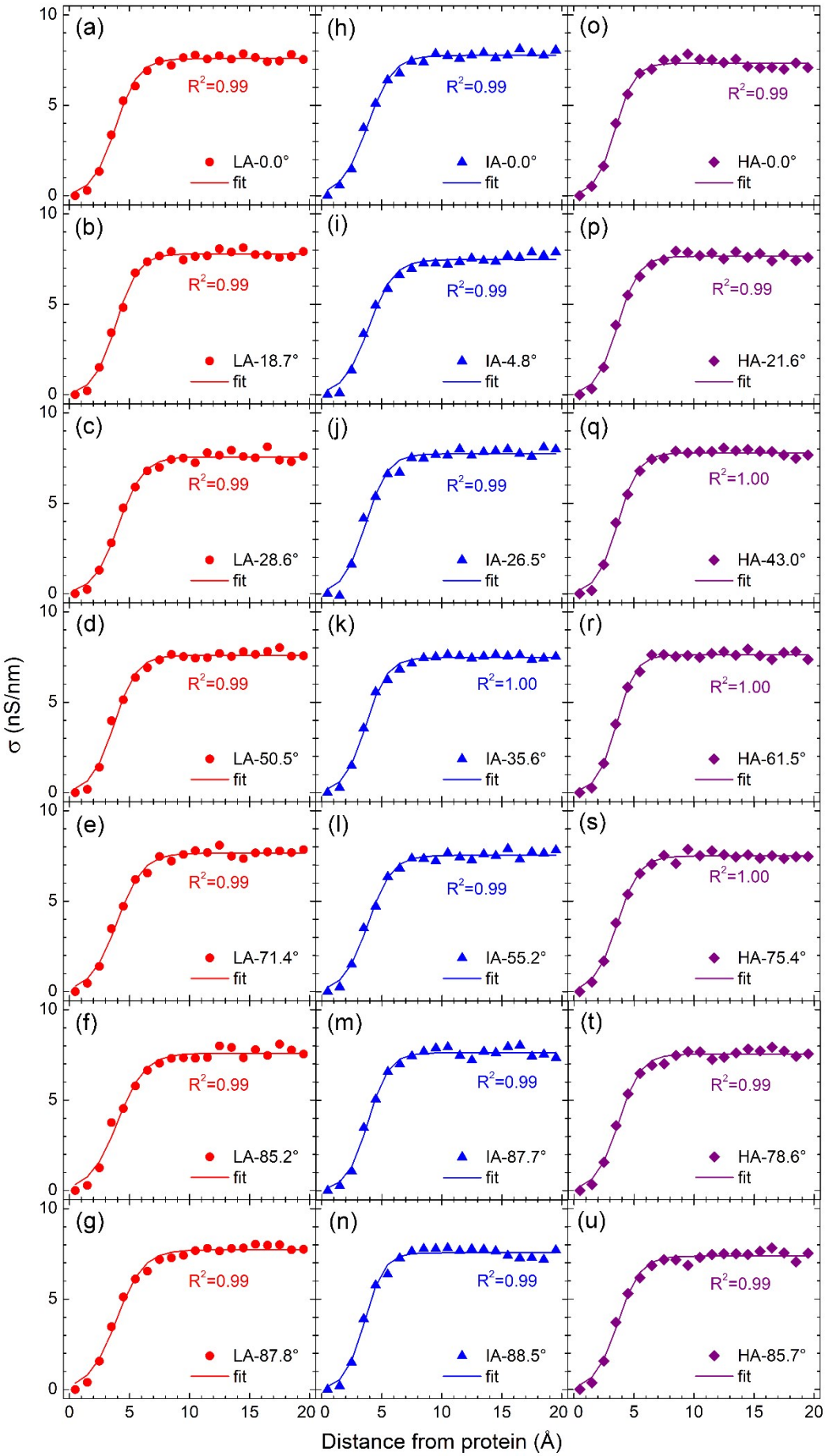
(a)
R²=0.99
LA-0.0°
fit
(h)
R²=0.99
IA-0.0°
fit
(o)
R²=0.99
HA-0.0°
fit
(b)
R²=0.99
LA-18.7°
fit
(i)
R²=0.99
IA-4.8°
fit
(p)
R²=0.99
HA-21.6°
fit
(c)
R²=0.99
LA-28.6°
fit
(j)
R²=0.99
IA-26.5°
fit
(q)
R²=1.00
HA-43.0°
fit
(d)
R²=0.99
LA-50.5°
fit
(k)
R²=1.00
IA-35.6°
fit
(r)
R²=1.00
HA-61.5°
fit
(e)
R²=0.99
LA-71.4°
fit
(l)
R²=0.99
IA-55.2°
fit
(s)
R²=1.00
HA-75.4°
fit
(f)
R²=0.99
LA-85.2°
fit
(m)
R²=0.99
IA-87.7°
fit
(t)
R²=0.99
HA-78.6°
fit
(g)
R²=0.99
LA-87.8°
fit
(n)
R²=0.99
IA-88.5°
fit
(u)
R²=0.99
HA-85.7°
fit
σ (nS/nm)
Distance from protein (Å)
0
5
10
15
20

Figure S8. Conductivity distributions around $\alpha_x\beta_2$ placed inside a 30-nm diameter nanopore at 50 mV/nm. Conductivities versus the distance from the protein surface for *LA* (**a-g**, *red lines*), *IA* (**h-n**, *blue lines*) or *HA* (**o-u**, *purple lines*) $\alpha_x\beta_2$ at different orientation angles. Data were acquired for seven orientations ranging from 0-90° from a 10-ns simulation each. The volume of electrolyte region was decomposed into serial 1-Å thick shells from the protein surface (**Supplementary Note 2**). The conductivity in each shell was calculated from a 10-ns simulation of 200 frames in 1 M KCl electrolyte. R^2 is the *R*-squared for each fitting.

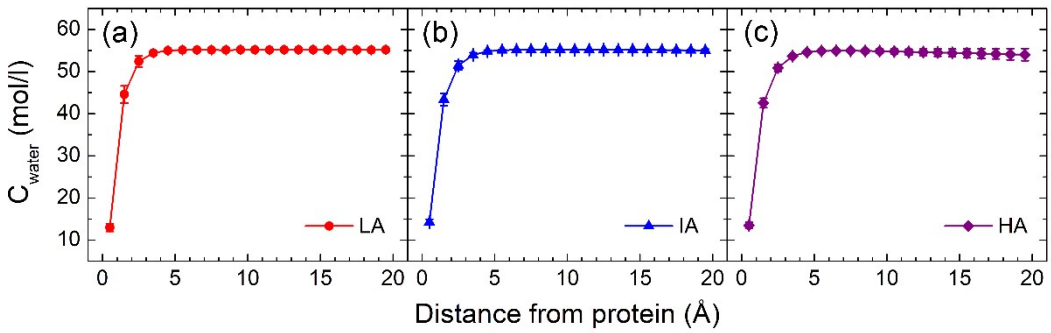

Figure S9. Dependence of the concentration of water molecules (C_{water}) in electrolyte on the distance from $\alpha_x\beta_2$ skeleton. (**a**) *LA* conformation, (**b**) *IA* conformation, (**c**) *HA* conformation. Error bars represent the SDs for all orientations under each conformation. Here C_{water} decreases sharply in the range of 0-4 Å. The calculation of water concentration was detailed in **Supplementary Note 2**.

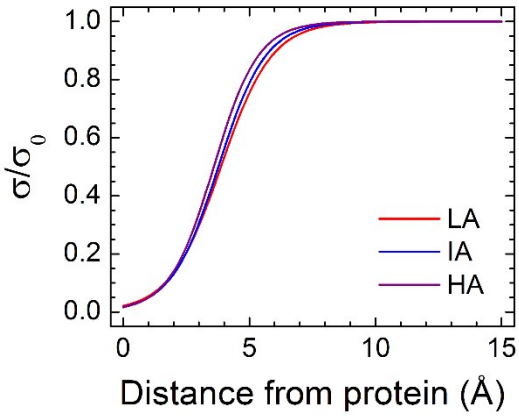

Figure S10. Dependence of the conductivity around three conformations of $\alpha_x\beta_2$ on the distance from the protein. Curves were depicted via Equation 5 with the fitted parameters a_p and b_p of three conformations in **Figure 3d**. The conductivities were normalized by the conductivity of bulk region σ_0.

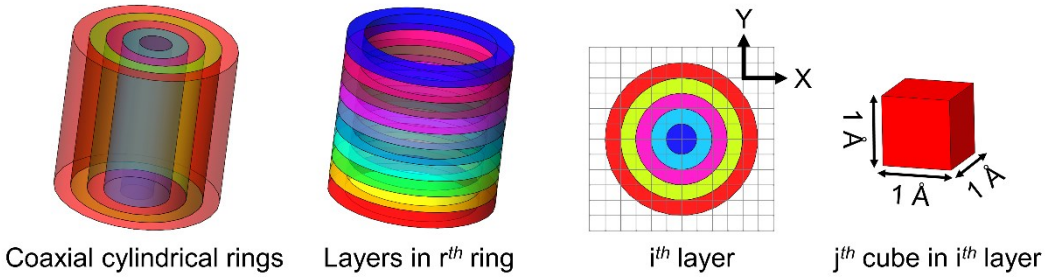

Figure S11. Schematics of the discrete model adopted from the literature 9. The nanopore was divided into successive coaxial cylindrical rings with a thickness of 1 Å (*left*). Each cylindrical ring was further segregated into sequential layers along *Z*-axis with a thickness of 1 Å (*second left*) and mapped into square meshes for discretization (*third left*). The conductivity in each cube (*right*) was determined by the radial distance from the pore surface and the nearest distance from the protein surface. The conductance of the nanopore was then obtained by summing all the cubic bins upon the serial-parallel integration (see "Discrete model" for details in **Supplementary Note 3**).

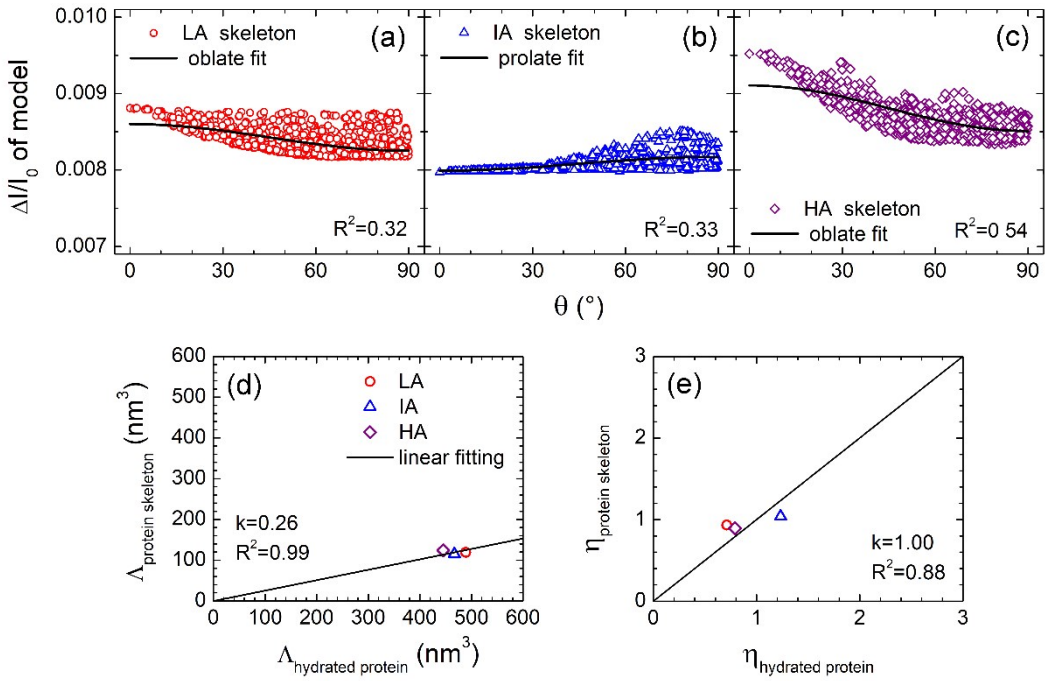

Figure S12. Spheroidal approximation of $\alpha_x\beta_2$ skeleton of three conformations via the relative blockade currents estimated from the discrete model in a 30-nm diameter nanopore at 50 mV/nm. The volume occupied by protein skeleton was considered as the discrete cubic meshes with null distance from the nearest protein surface in the discrete model. The modeled currents only accounted for the conductance of protein skeleton but not hydration shell. (**a-c**) Relative blockade currents $\Delta I/I_0$ of 1000 randomly-oriented *LA* (**a**, *circles*), *IA* (**b**, *triangles*) or *HA* (**c**, *diamonds*) skeletons generated by the discrete model. The curves were obtained by an oblate (**a**), a prolate (**b**) or an oblate (**c**) fitting, respectively, using Equations S1-S6. (**d**) Comparisons of approximate spheroidal volumes of the protein skeletons and the hydrated proteins. The *solid line* is the linear fitting with a slope of k and a determination coefficient of R^2. (**e**) Similar comparisons in panel **d** but for the length-to-diameter ratios η.

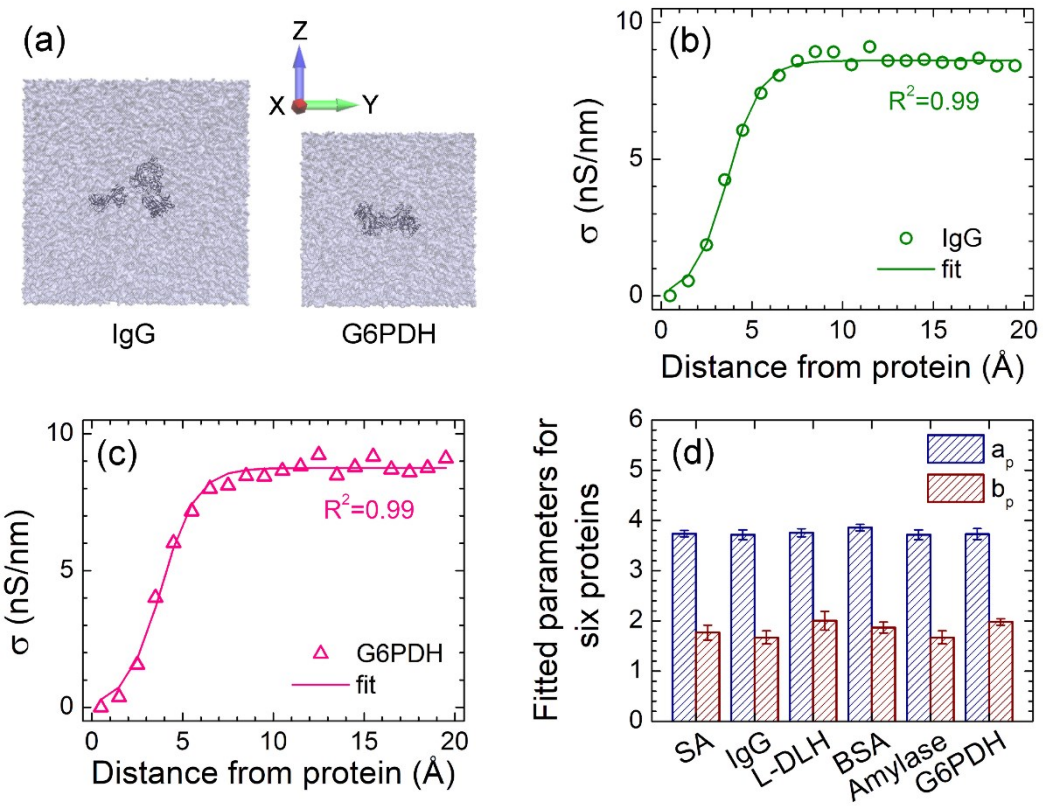

Figure S13. MD simulations of different proteins in periodic electrolyte cubic boxes. (**a**) Schematics of MD simulation systems for typical proteins. An *IgG* (*left*) or a *G6PDH* (*right*) molecule was dissolved in a 24.6 or 19.6-nm electrolyte cubic box. Other four proteins (*SA*, *L-DLH*, *BSA* or *Amylase*) were also dissolved in the 19.6-nm cube (*not shown*). The 1 M KCl aqueous box was colored with semitransparent *iceblue* and the protein in the box was colored in *black*. (**b**, **c**) Conductivity distributions around *IgG* and *G6PDH* placed inside a periodic electrolyte cube depicted in panel **a** at 50 mV/nm, respectively. Volume surrounding the protein was partitioned into sequential shells spaced by 1 Å-thick intervals from the protein surface. The conductivity in each shell was calculated from a 10-ns simulation of 200 frames in 1 M KCl electrolyte. R^2 is the *R*-squared for each fitting. The fitted curves for other four proteins are not shown here. (**d**) Parameters a_p and b_p were averaged from three independent simulations at 50 mV/nm. Error bars are SDs. The mean values and SDs of the fitted parameters of the six proteins are a_p=3.74±0.06 and b_p=1.87±0.13.

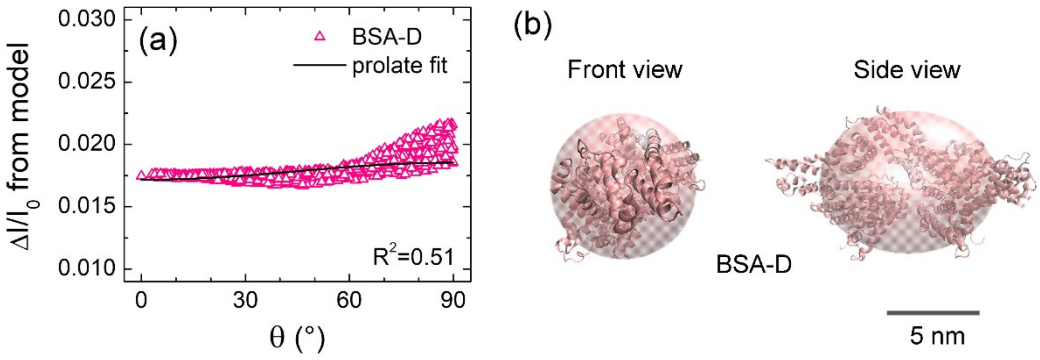

Figure S14. **Prediction of bovine serum albumin dimer (*BSA-D*) by the discrete model using the approximate spheroid in a 30-nm diameter nanopore filled with 1 M KCl at 50 mV/nm.** (**a**) Correlation between relative blockade currents $\Delta I/I_0$ and relevant orientation angles θ of *BSA-D*. *Pink triangle* were generated from 1000 random orientations by the discrete model and *black curve* represents the fitting of spheroidal approximation by Equations S1-S6. R^2 is the *R*-squared. (**b**) Comparison of the predicted ellipsoid of *BSA-D* with its crystal structure from Protein Data Bank (PDB code: 3V03), and the accurate shape values are shown in **Table S3**.

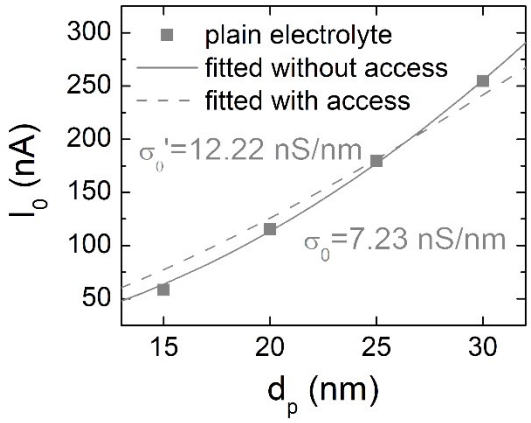

Figure S15. Effect of access resistance on the pore diameter dependence of ionic current in the nanopore filled with plain electrolyte alone. *Gray squares* and *solid line* are the data points and the fitted line replicated from **Figure S3e**. The fitted conductivity σ_0 via Equation 1 which does not contain the access resistance is 7.23 nS/nm. *Dashed line* was computed from the fitting of $I_0=\sigma'_0\pi d_p^2El/4(l+0.8d_p)$, which contains two access resistances in the inlet and outlet of the nanopore [2, 6, 14-16] and yielded the fitted conductivity σ'_0 of 12.22 nS/nm. Since the conductivity of the plain electrolyte in nanopore is 7-8 nS/nm (**Figures S6-S8**), Equation 1 without access resistance is applicable, indicating that there is no apparent access resistance in our MD systems.

Supplementary Tables

Table S1. The fitted parameters for two approximate spheroids of each conformation of $\alpha_x\beta_2$ via MD data.

`Conformations[|]	Spheroids	*A* (nm)	*B* (nm)	$R^{2\dagger}$	Λ (nm^3)	*A*/*B*	$f_{min}^{\ddagger}$	$f_{max}^{\ddagger}$
LA	prolate	14.3	8.1	0.53	494.9	1.76	1.25	1.67
	oblate□	7.2	11.0	0.67	459.3	0.65	1.38	1.83
IA	prolate□	15.7	7.6	0.81	469.8	2.08	1.20	1.72
	oblate	6.4	11.3	0.70	429.2	0.56	1.34	1.97
HA	prolate	12.7	8.6	0.44	486.6	1.49	1.31	1.62
	oblate□	7.9	10.6	0.62	468.9	0.74	1.41	1.71

[|]: *LA*, low-affinity state; *IA*, intermediate-affinity state; *HA*, high-affinity state.

[†]: determination coefficient (*R*-squared).

[‡]: Minimal and maximal electrical shape factors.

□: Optimal shape with higher *R*-squared value in the spheroidal approximation.

Table S2. The fitted parameters for two approximate spheroids of six proteins via the currents from discrete model.

Proteins[|]	Spheroids	A (nm)	B (nm)	$R^{2\dagger}$	Λ (nm^3)	A/B	f_{min}[‡]	f_{max}[‡]
SA	prolate	5.7	5.6	0.03	94.2	1.02	1.49	1.51
	oblate□	5.4	5.8	0.29	94.3	0.94	1.49	1.51
IgG	prolate	7.6	7.6	0.01	231.8	1.00	1.50	1.50
	oblate□	6.9	8.0	0.14	232.7	0.86	1.46	1.60
L-LDH	prolate	8.3	7.5	0.26	247.4	1.11	1.44	1.53
	oblate□	7.0	8.2	0.81	245.9	0.86	1.46	1.60
BSA	prolate	6.5	6.2	0.23	133.1	1.04	1.48	1.51
	oblate□	6.1	6.5	0.43	133.0	0.94	1.48	1.54
Amylase	prolate□	6.0	5.5	0.65	95.0	1.09	1.45	1.53
	oblate	5.4	5.8	0.27	94.1	0.94	1.48	1.54
G6PDH	prolate□	8.7	6.6	0.56	200.3	1.31	1.36	1.58
	oblate	6.9	7.4	0.05	201.7	0.93	1.48	1.54
BSA-D	prolate□	9.2	7.4	0.51	262.0	1.24	1.39	1.56
	oblate	6.9	8.4	0.40	256.7	0.83	1.44	1.63

[|]: streptavidin (*SA*), anti-biotin immunoglobulin G1 (*IgG*), L-lactate dehydrogenase (*L-LDH*), bovine serum albumin (*BSA*), α-amylase (*Amylase*), glucose-6-phosphate dehydrogenase (*G6PDH*), *BSA* dimer (*BSA-D*)

[†]: *R*-squared.

[‡]: Minimal and maximal electrical shape factors.

□: Optimal shape with higher *R*-squared value in the spheroidal approximation. Since the *A/B* value of *SA* is closest to 1 for two types of spheroids, *SA* was also considered as a spherical shape in **Figure 5**.

Table S3. Comparisons of the volume Λ and length-to-diameter ratio $\eta = A/B$ of six proteins determined by the theoretical model and the reported experiments.

Proteins	Experiment		Theoretical model		Reference
	Λ (nm^3)	η	Λ (nm^3)	η	
SA	110±25	1	94.3	0.94	13
IgG	263±51	0.23±0.11	232.7	0.86	13
L-LDH	267	0.54	245.9	0.86	13
BSA	101±13	0.50±0.03	133.0	0.94	13
Amylase	99	1.5	95.0	1.09	13
G6PDH	220±9	2.3±0.1	200.3	1.31	13
BSA-D	260	2†	262.0	1.24	17

†: Estimated from the crystal structure (PDB code: 3V03).

References

1. D. C. Golibersuch, *Biophys. J.*, 1973, **13**, 265-280.
2. D. C. Golibersuch, *J. Appl. Phys.*, 1973, **44**, 2580-2584.
3. J. A. Osborn, *Physical Review*, 1945, **67**, 351-357.
4. N. B. Grover, J. Naaman, Bensasso.S and F. Doljanski, *Biophys. J.*, 1969, **9**, 1398.
5. Z. P. Qin, J. A. Zhe and G. X. Wang, *Meas. Sci. Technol.*, 2011, **22**, 045804.
6. R. W. Deblois and C. P. Bean, *Rev. Sci. Instrum.*, 1970, **41**, 909.
7. R. W. Deblois, C. P. Bean and R. K. A. Wesley, *J. Colloid Interface Sci.*, 1977, **61**, 323-335.
8. W. R. Smythe, *Phys. Fluids*, 1964, **7**, 633-638.
9. W. Si and A. Aksimentiev, *ACS Nano*, 2017, **11**, 7091-7100.
10. A. Aksimentiev, *Nanoscale*, 2010, **2**, 468-483.
11. M. Belkin and A. Aksimentiev, *ACS Appl. Mater. Interfaces*, 2016, **8**, 12599-12608.
12. R. M. M. Smeets, U. F. Keyser, D. Krapf, M. Y. Wu, N. H. Dekker and C. Dekker, *Nano Lett.*, 2006, **6**, 89-95.
13. E. C. Yusko, B. R. Bruhn, O. M. Eggenberger, J. Houghtaling, R. C. Rollings, N. C. Walsh, S. Nandivada, M. Pindrus, A. R. Hall, D. Sept, J. L. Li, D. S. Kalonia and M. Mayer, *Nat. Nanotechnol.*, 2017, **12**, 360-367.
14. J. E. Hall, *J. Gen. Physiol.*, 1975, **66**, 531-532.
15. S. W. Kowalczyk, A. Y. Grosberg, Y. Rabin and C. Dekker, *Nanotechnology*, 2011, **22**, 315101.
16. I. Vodyanoy and S. M. Bezrukov, *Biophys. J.*, 1992, **62**, 10-11.
17. L. Z. Wu, H. Liu, W. Y. Zhao, L. Wang, C. R. Hou, Q. J. Liu and Z. H. Lu, *Nanoscale Res. Lett.*, 2014, **9**, 10.